Concentration instability of sedimenting spheres in a second-order fluid

Ramanathan Vishnampet and David Saintillan[a)]
Department of Mechanical Science and Engineering, University of Illinois at Urbana-Champaign, Urbana, Illinois 61801, USA

The slow sedimentation of a dilute suspension of spherical particles in a second-order fluid is investigated using theory and numerical simulations. We first analyze the motion of a single isolated spherical particle sedimenting under gravity when placed in a linear flow field. In the limit of weak viscoelasticity (low Deborah number), the velocity of the particle is calculated, and the nonlinear coupling of the settling motion with the local flow field is shown to result in a lateral drift in a direction perpendicular to gravity. By the same effect, the mean flow driven by weak horizontal density fluctuations in a large-scale suspension of hydrodynamically interacting particles will also result in a horizontal drift, which has the effect of reinforcing the fluctuations as we demonstrate using a linear stability analysis. Based on this mechanism, an initially homogeneous suspension is expected to develop concentration fluctuations, a prediction supported by previous experiments on sedimentation in polymeric liquids. We further confirm this prediction using large-scale weakly nonlinear numerical simulations based on a point-particle model. Concentration fluctuations are indeed found to grow in the simulations, and are shown to result in an enhancement of the mean settling speed and velocity fluctuations compared to the Newtonian case. © *2012 American Institute of Physics*. [http://dx.doi.org/10.1063/1.4733700]

I. INTRODUCTION

The sedimentation of small particles suspended in a fluid is a ubiquitous phenomenon arising in both natural and industrial processes.[1] It has received much attention over the last few decades, and several central questions, such as the mechanisms controlling the magnitude of velocity fluctuations, remain controversial to date.[2–13] While the vast majority of previous investigations has focused on the case of suspensions in Newtonian fluids, numerous industrial applications involving sedimentation, notably in the chemical engineering field, use suspending fluids such as polymer solutions in which non-Newtonian effects may become important. A few experimental studies in viscoelastic fluids show that the dynamics in these systems differ significantly from the Newtonian case,[14–22] emphasizing the need for a better understanding of non-Newtonian effects in sedimenting suspensions.

In recent experiments, Mora *et al.*[21] considered the case of a dilute suspension of monodisperse non-Brownian spheres sedimenting in a polymer solution. Starting from well-mixed homogeneous suspensions, they reported the formation of particle-rich structures taking the form of vertical columns surrounded by regions of clear fluid. This pattern formation, also observed in previous studies using other types of fluids,[15,18] resulted in an enhancement of the settling velocity beyond the velocity of an isolated particle. These findings come in stark contrast to what is typically observed in Newtonian fluids, where suspensions remain homogeneous and exhibit velocity hindering. Mora *et al.*[21] explained this phenomenon as a result of local clustering of nearby particles, which is known to occur in viscoelastic and shear-thinning fluids.[19,20,23–25] It is not entirely clear, however, how

---

a)Electronic mail: dstn@illinois.edu.

local clustering can lead to the formation of macroscopic structures of the type observed in full-scale suspensions.

Other types of sedimenting suspensions are known to develop large-scale inhomogeneities. Suspensions of non-spherical or non-rigid particles in Newtonian fluids are subject to concentration instabilities as a result of hydrodynamic interactions, also leading to the formation of large-scale concentrated structures.[26–38] These instabilities can be explained as a consequence of a coupling between the anisotropic mobility of the particles and the macroscale flow field generated by the density fluctuations in the suspension:[26,32] specifically, density fluctuations create a disturbance flow which causes the particles to orient or deform in such a way that they migrate toward the regions of higher concentration. This mechanism, however, does not apply to isotropic particles (such as rigid spheres) in Newtonian fluids, as their mobility is unaffected by the local flow field, a direct consequence of the linearity of Stokes flow. Yet, in the case of a viscoelastic fluid, a coupling between settling motion and local fluid flow is possible even for spheres owing to nonlinearities, and this suggests that an instability similar to that for anisotropic particles may also exist in this case. Elucidating this coupling and its implications for suspension stability is the subject of the present work.

In a recent study, Phillips[39] proposed a theoretical model for this instability. He considered the effect of pair particle interactions (calculated for two identical spheres in the case of a second-order fluid[24]) on the evolution of density fluctuations in a suspension of particles with a concentration profile initially perturbed in the horizontal direction. He found that particle–particle interactions can lead to an effective flux which competes with diffusion and can result in the formation of dense vertical columns. The model we propose herein describes the same effect but from a different perspective: we show that the horizontal migration causing the amplification of density fluctuations can be interpreted as a consequence of the nonlinear interaction of the settling motion of the particles under gravity with the large-scale mean-field fluid velocity driven by density fluctuations across the suspension. We also confirm the predictions of our theoretical model by performing weakly nonlinear particle simulations using a point-particle model.

In the following, we focus on the case of a second-order fluid, which is amenable to analytical solutions while capturing sufficient physics to illustrate the general effects of viscoelasticity on the dynamics. The paper is organized as follows. The constitutive model and its conditions of validity are described in Sec. II A. In Sec. II B, we analyze the nonlinear coupling that occurs when a single sphere sediments in an imposed linear flow, and derive a correction to the Newtonian mobility as a function of the local velocity gradient. This correction is then used to study the linear stability of a homogeneous suspension in Sec. II D, where an instability similar to that for anisotropic particles is predicted. To analyze the instability in finite systems beyond the linear regime, we also describe results from numerical simulations of large-scale suspensions in Sec. III. Implications and limitations of the model and simulations are discussed in Sec. IV.

II. THEORY

A. Constitutive relation and non-dimensionalization

In this work, we specifically consider the case of a second-order fluid, which corresponds to an asymptotic expansion of the Oldroyd-B model for weak viscoelasticity (as measured by the Deborah number defined below) and slowly varying flows.[40] For a flow with velocity field $\mathbf{u}$ and pressure field p, the stress tensor is written as the sum of Newtonian and non-Newtonian contributions:

$$\boldsymbol{\sigma} = -p\mathbf{I} + 2\eta_0 \mathbf{E} + \boldsymbol{\Sigma}(\mathbf{u}). \tag{1}$$

In Eq. (1), η_0 denotes the zero-shear-rate (or Newtonian) viscosity, $\mathbf{E} = (\nabla\mathbf{u} + \nabla\mathbf{u}^T)/2$ is the rate-of-strain tensor, and $\boldsymbol{\Sigma}(\mathbf{u})$ is the nonlinear polymeric extra stress given by

$$\boldsymbol{\Sigma}(\mathbf{u}) = -\Psi_1 \overset{\triangledown}{\mathbf{E}} + 4\Psi_2 \mathbf{E} \cdot \mathbf{E}, \tag{2}$$

where $\Psi_1 > 0$ and $\Psi_2 < 0$ are the first and second normal stress coefficients, and where the first term on the right-hand side involves the upper-convected derivative of the rate-of-strain tensor:

$$\overset{\triangledown}{\mathbf{E}} = \frac{\partial \mathbf{E}}{\partial t} + \mathbf{u} \cdot \nabla \mathbf{E} - (\nabla \mathbf{u}^T \cdot \mathbf{E} + \mathbf{E} \cdot \nabla \mathbf{u}). \tag{3}$$

Stresses may be non-dimensionalized by $\eta_0 \dot{\gamma}$ where $\dot{\gamma}$ is a characteristic shear rate for the flow of interest. We introduce the Deborah number (or dimensionless flow strength) $\text{De} = \Psi_1 \dot{\gamma} / \eta_0$ and the ratio of the normal stress coefficients $\lambda = -4\Psi_2/\Psi_1$, and we note that the second-order fluid model is valid for $\text{De} \ll 1$. The dimensionless stress tensor is then written as $\boldsymbol{\sigma} = -p\mathbf{I} + 2\mathbf{E} + \text{De}\,\boldsymbol{\Sigma}(\mathbf{u})$, where the polymeric stress is now given by

$$\boldsymbol{\Sigma}(\mathbf{u}) = -\left[\overset{\triangledown}{\mathbf{E}} + \lambda \mathbf{E} \cdot \mathbf{E} \right]. \tag{4}$$

In the problem considered here, two different characteristic shear rates may be identified. The first one corresponds to the shear rate created by a sedimenting sphere on the scale of the particle and may be estimated as the ratio of the Stokes velocity U_s by the radius a of a sphere: $\dot{\gamma} = U_s/a = F/6\pi\eta_0 a^2$ where F is the magnitude of the gravitational force acting on a particle. The second one corresponds to the macroscopic flow U_0 created by the density fluctuations on the scale L of the suspension: $\dot{\gamma} = U_0/L$, where the velocity scale U_0 depends on the particle distribution in the suspension and will be defined more precisely in Sec. II D. In the following, we assume that both characteristic shear rates are such that the corresponding Deborah numbers are much less than unity.

B. Isolated sphere sedimenting in a linear flow field

We first analyze the case of a single isolated sphere of radius a, surface S, and outward normal $\mathbf{n}$ sedimenting under the gravitational force $\mathbf{F}$ in a linear velocity field of the form $\mathbf{V}(\mathbf{x}) = \mathbf{V}_0 + \mathbf{x} \cdot \mathbf{A}$, where $\mathbf{A} = \nabla \mathbf{V}$ is the imposed velocity gradient. Also denote by Q and $\mathbf{S}$ the associated pressure and stress fields, respectively. For ease of analysis, the position vector $\mathbf{x}$ is defined such that the sphere is located at the origin. In this section, the characteristic shear rate $\dot{\gamma}$ used for non-dimensionalization is taken to be the magnitude of the imposed velocity gradient: $\dot{\gamma} = (\mathbf{A}{:}\mathbf{A})^{1/2}$, and lengths are made dimensionless using the particle radius a.

When sedimenting in this flow field, the sphere will assume a translational velocity $\mathbf{U}_p$ and an angular velocity $\boldsymbol{\Omega}_p$. In a Newtonian fluid, it is a well-known result that $\mathbf{U}_p$ is given as the sum of the Stokes velocity and of the mean external velocity:

$$\mathbf{U}_p = \mathbf{U}_s + \mathbf{V}_0. \tag{5}$$

Here, we wish to determine the first non-Newtonian correction to $\mathbf{U}_p$ in the limit of $\text{De} \ll 1$. This correction may be obtained using a classical method based on the Lorentz reciprocal theorem,[41–43] which we outline here.

Denoting by $\mathbf{u}$ and p the total velocity and pressure fields in the fluid, the dynamics are governed by the momentum and continuity equations:

$$\nabla \cdot \boldsymbol{\sigma} = \mathbf{0}, \quad \nabla \cdot \mathbf{u} = 0, \tag{6}$$

where $\boldsymbol{\sigma} = -p\mathbf{I} + 2\mathbf{E} + \text{De}\,\boldsymbol{\Sigma}(\mathbf{u})$ and the polymeric stress $\boldsymbol{\Sigma}(\mathbf{u})$ is again given by Eq. (4). In addition, the boundary conditions for the velocity field are

$$\mathbf{u}(\mathbf{x}) = \mathbf{U}_p + \boldsymbol{\Omega}_p \times \mathbf{x} \quad \text{as } \mathbf{x} \in S, \tag{7}$$

$$\mathbf{u}(\mathbf{x}) \rightarrow \mathbf{V}(\mathbf{x}) \quad \text{as } |\mathbf{x}| \rightarrow \infty, \tag{8}$$

and the force and torque balances on the sphere read as

$$\int_S \boldsymbol{\sigma} \cdot \mathbf{n}\, dS = \mathbf{F}, \quad \int_S \mathbf{x} \times (\boldsymbol{\sigma} \cdot \mathbf{n})\, dS = \mathbf{0}. \tag{9}$$

For convenience, we also define disturbance flow variables $\hat{\mathbf{u}}$, $\hat{p}$, and $\hat{\boldsymbol{\sigma}}$, obtained by subtracting the imposed flow variables from $\mathbf{u}$, p, and $\boldsymbol{\sigma}$:

$$\hat{\mathbf{u}}(\mathbf{x}) = \mathbf{u}(\mathbf{x}) - \mathbf{V}(\mathbf{x}), \tag{10}$$

$$\hat{p}(\mathbf{x}) = p(\mathbf{x}) - Q(\mathbf{x}), \tag{11}$$

$$\hat{\boldsymbol{\sigma}}(\mathbf{x}) = \boldsymbol{\sigma}(\mathbf{x}) - \mathbf{S}(\mathbf{x}). \tag{12}$$

These perturbation variables still satisfy the continuity equation $\nabla \cdot \hat{\mathbf{u}} = 0$ and momentum equation $\nabla \cdot \hat{\boldsymbol{\sigma}} = \mathbf{0}$, where the disturbance stress tensor is now expressed as

$$\hat{\boldsymbol{\sigma}} = -\hat{p}\,\mathbf{I} + 2\hat{\mathbf{E}} + \mathrm{De}\left[\boldsymbol{\Sigma}(\hat{\mathbf{u}} + \mathbf{V}) - \boldsymbol{\Sigma}(\mathbf{V})\right], \tag{13}$$

and the boundary conditions Eqs. (7) and (8) become

$$\hat{\mathbf{u}}(\mathbf{x}) = \mathbf{U}_p + \boldsymbol{\Omega}_p \times \mathbf{x} - \mathbf{V}(\mathbf{x}) \quad \text{as} \ \ \mathbf{x} \in S, \tag{14}$$

$$\hat{\mathbf{u}}(\mathbf{x}) \to \mathbf{0} \quad \text{as} \ \ |\mathbf{x}| \to \infty. \tag{15}$$

We wish to solve the disturbance problem in the asymptotic limit of weak viscoelasticity, or $\mathrm{De} \ll 1$. As it is a regular perturbation problem, we may assume the following expansion for the disturbance velocity:

$$\hat{\mathbf{u}} = \hat{\mathbf{u}}^{(0)} + \mathrm{De}\,\hat{\mathbf{u}}^{(1)} + \cdots, \tag{16}$$

with similar expansions for the disturbance pressure $\hat{p}$ and stress tensor $\hat{\boldsymbol{\sigma}}$, as well as for the particle linear and angular velocities $\mathbf{U}_p$ and $\boldsymbol{\Omega}_p$:

$$\hat{p} = \hat{p}^{(0)} + \mathrm{De}\,\hat{p}^{(1)} + \cdots, \tag{17}$$

$$\hat{\boldsymbol{\sigma}} = \hat{\boldsymbol{\sigma}}^{(0)} + \mathrm{De}\,\hat{\boldsymbol{\sigma}}^{(1)} + \cdots, \tag{18}$$

$$\mathbf{U}_p = \mathbf{U}_p^{(0)} + \mathrm{De}\,\mathbf{U}_p^{(1)} + \cdots, \tag{19}$$

$$\boldsymbol{\Omega}_p = \boldsymbol{\Omega}_p^{(0)} + \mathrm{De}\,\boldsymbol{\Omega}_p^{(1)} + \cdots. \tag{20}$$

1. Zeroth-order problem

The zeroth-order problem corresponds to the Newtonian case, and is formally obtained by setting $\mathrm{De} \equiv 0$ in the governing equations. Specifically, the dynamics are governed by the momentum and continuity equations,

$$\nabla \cdot \hat{\boldsymbol{\sigma}}^{(0)} = \mathbf{0}, \quad \nabla \cdot \hat{\mathbf{u}}^{(0)} = 0, \tag{21}$$

where $\hat{\boldsymbol{\sigma}}^{(0)} = -\hat{p}^{(0)}\mathbf{I} + \nabla\hat{\mathbf{u}}^{(0)} + \nabla\hat{\mathbf{u}}^{(0)T}$, subject to the boundary conditions

$$\hat{\mathbf{u}}^{(0)}(\mathbf{x}) = \mathbf{U}_p^{(0)} + \boldsymbol{\Omega}_p^{(0)} \times \mathbf{x} - \mathbf{V}(\mathbf{x}) \quad \text{as} \ \ \mathbf{x} \in S, \tag{22}$$

$$\hat{\mathbf{u}}^{(0)}(\mathbf{x}) \to \mathbf{0} \quad \text{as} \ \ |\mathbf{x}| \to \infty, \tag{23}$$

and to the force and torque balance of Eq. (9).

The solution is classic, and may be obtained for instance using the method of harmonic expansions.[44] In particular, the disturbance velocity field $\hat{\mathbf{u}}^{(0)}$ has contributions from both the gravitational force and the external linear flow:

$$\hat{\mathbf{u}}^{(0)}(\mathbf{x}) = \frac{1}{8\pi}\left[\left(\frac{\mathbf{I}}{x} + \frac{\mathbf{xx}}{x^3}\right) + \frac{1}{3}\left(\frac{\mathbf{I}}{x^3} - 3\frac{\mathbf{xx}}{x^5}\right)\right] \cdot \mathbf{F} + \left[-\frac{5}{4}\frac{\mathbf{xxx}}{x^5} - \frac{1}{2}\left(\frac{\mathbf{Ix}}{x^5} - \frac{5}{2}\frac{\mathbf{xxx}}{x^7}\right)\right] : (\mathbf{A} + \mathbf{A}^T). \tag{24}$$

The linear velocity of the sphere is obtained as the sum of the Newtonian Stokes velocity and of the local external velocity, and its angular velocity is half the imposed vorticity:

$$\mathbf{U}_p^{(0)} = \frac{\mathbf{F}}{6\pi} + \mathbf{V}_0, \quad \mathbf{\Omega}_p^{(0)} = \frac{1}{2}\nabla \times \mathbf{V}. \tag{25}$$

2. First-order problem

Having solved the Newtonian problem, we then attempt to obtain a solution to $O(\text{De})$. The first-order problem also satisfies the momentum and continuity equations:

$$\nabla \cdot \hat{\boldsymbol{\sigma}}^{(1)} = \mathbf{0}, \quad \nabla \cdot \hat{\mathbf{u}}^{(1)} = 0, \tag{26}$$

where the stress tensor is now given by

$$\hat{\boldsymbol{\sigma}}^{(1)} = -\hat{p}^{(1)}\mathbf{I} + \nabla\hat{\mathbf{u}}^{(1)} + \nabla\hat{\mathbf{u}}^{(1)T} + \boldsymbol{\Sigma}(\hat{\mathbf{u}}^{(0)} + \mathbf{V}) - \boldsymbol{\Sigma}(\mathbf{V}). \tag{27}$$

Note that the disturbance velocity $\hat{\mathbf{u}}$ may be replaced by $\hat{\mathbf{u}}^{(0)}$ to order $O(\text{De})$ in the nonlinear component of the stress. The boundary conditions for this problem are

$$\hat{\mathbf{u}}^{(1)}(\mathbf{x}) = \mathbf{U}_p^{(1)} + \mathbf{\Omega}_p^{(1)} \times \mathbf{x} \quad \text{as } \mathbf{x} \in S, \tag{28}$$

$$\hat{\mathbf{u}}^{(1)}(\mathbf{x}) \to \mathbf{0} \quad \text{as } |\mathbf{x}| \to \infty, \tag{29}$$

and the force and torque balances simplify as

$$\int_S \hat{\boldsymbol{\sigma}}^{(1)} \cdot \mathbf{n}\, dS = \mathbf{0}, \quad \int_S \mathbf{x} \times (\hat{\boldsymbol{\sigma}}^{(1)} \cdot \mathbf{n})\, dS = \mathbf{0}. \tag{30}$$

To determine the particle linear motion $\mathbf{U}_p^{(1)}$, we make use of the Lorentz reciprocal theorem.[43,45] Consider a complementary Newtonian flow problem with velocity $\mathbf{v}$, pressure q, and stress $\mathbf{s}$, that satisfies

$$\nabla \cdot \mathbf{s} = \mathbf{0}, \quad \nabla \cdot \mathbf{v} = 0, \tag{31}$$

with $\mathbf{s} = -q\mathbf{I} + \nabla\mathbf{v} + \nabla\mathbf{v}^T$, subject to the boundary conditions

$$\mathbf{v}(\mathbf{x}) = \mathbf{e} \quad \text{as } \mathbf{x} \in S, \tag{32}$$

$$\mathbf{v}(\mathbf{x}) \to \mathbf{0} \quad \text{as } |\mathbf{x}| \to \infty, \tag{33}$$

where $\mathbf{e}$ is an arbitrary fixed vector. The solution of this complementary problem is straightforward and given by

$$\mathbf{v}(\mathbf{x}) = \frac{3}{4}\left[\left(\frac{\mathbf{I}}{x} + \frac{\mathbf{xx}}{x^3}\right) + \frac{1}{3}\left(\frac{\mathbf{I}}{x^3} - 3\frac{\mathbf{xx}}{x^5}\right)\right] \cdot \mathbf{e}. \tag{34}$$

Using the momentum equations for $\hat{\boldsymbol{\sigma}}^{(1)}$ and $\mathbf{s}$ and using the symmetry of the stress tensors, we can derive the following expressions:

$$\nabla \cdot (\hat{\boldsymbol{\sigma}}^{(1)} \cdot \mathbf{v}) = \hat{\boldsymbol{\sigma}}^{(1)}{:}(\nabla\mathbf{v} + \nabla\mathbf{v}^T)/2, \tag{35}$$

$$\nabla \cdot (\mathbf{s} \cdot \hat{\mathbf{u}}^{(1)}) = \mathbf{s}{:}(\nabla\hat{\mathbf{u}}^{(1)} + \nabla\hat{\mathbf{u}}^{(1)T})/2. \tag{36}$$

Subtracting Eq. (36) from Eq. (35), integrating over the entire volume of fluid V_f, and using the divergence theorem then yields:

$$-\int_S \mathbf{n} \cdot [\hat{\boldsymbol{\sigma}}^{(1)} \cdot \mathbf{v} - \mathbf{s} \cdot \hat{\mathbf{u}}^{(1)}]dS = \frac{1}{2}\int_{V_f}[\hat{\boldsymbol{\sigma}}^{(1)} : (\nabla\mathbf{v} + \nabla\mathbf{v}^T) - \mathbf{s} : (\nabla\hat{\mathbf{u}}^{(1)} + \nabla\hat{\mathbf{u}}^{(1)T})]dV. \tag{37}$$

Note that $\mathbf{v} = \mathbf{e}$ and $\hat{\mathbf{u}}^{(1)} = \mathbf{U}_p^{(1)} + \mathbf{\Omega}_p^{(1)} \times \mathbf{x}$ on the surface S of the sphere, and that the stress tensor for the complementary problem is known. Using the force balance Eq. (30), we therefore simplify the left-hand side in Eq. (37) as

$$-\int_S \mathbf{n} \cdot [\hat{\boldsymbol{\sigma}}^{(1)} \cdot \mathbf{v} - \mathbf{s} \cdot \hat{\mathbf{u}}^{(1)}]dS = -6\pi \, \mathbf{U}_p^{(1)} \cdot \mathbf{e}. \tag{38}$$

The right-hand side in Eq. (37) may also be simplified by substituting Eq. (27) for the expression of $\hat{\boldsymbol{\sigma}}^{(1)}$ and making use of the continuity equations for $\hat{\mathbf{u}}^{(1)}$ and $\mathbf{v}$. After manipulation, Eq. (37) yields the following expression, valid for any vector $\mathbf{e}$:

$$\mathbf{U}_p^{(1)} \cdot \mathbf{e} = -\frac{1}{12\pi} \int_{V_f} \left[\mathbf{\Sigma}(\hat{\mathbf{u}}^{(0)} + \mathbf{V}) - \mathbf{\Sigma}(\mathbf{V}) \right] : (\nabla \mathbf{v} + \nabla \mathbf{v}^T)dV. \tag{39}$$

As $\hat{\mathbf{u}}^{(0)}$ and $\mathbf{v}$ are known from Eqs. (24) and (34), this may be used to determine $\mathbf{U}_p^{(1)}$. The evaluation of the integral in Eq. (39) is cumbersome but can be performed analytically. All calculations done, we find:

$$\mathbf{U}_p^{(1)} = \frac{1}{35}(\mathbf{A} + \mathbf{A}^T) \cdot \mathbf{V}_0 + \frac{1}{6\pi} \left[f_1(\lambda)\mathbf{A} + f_2(\lambda)\mathbf{A}^T \right] \cdot \mathbf{F}, \tag{40}$$

where the two parameters $f_1(\lambda)$ and $f_2(\lambda)$ are functions of the ratio of the normal stress coefficients:

$$f_1(\lambda) = \frac{\lambda}{8} + \frac{5}{64}, \quad f_2(\lambda) = \frac{\lambda}{8} - \frac{11}{64}. \tag{41}$$

In dimensional variables, the total settling velocity of the sphere can therefore be written

$$\mathbf{U}_p = \mathbf{M}_1(\mathbf{A}) \cdot \mathbf{V}_0 + \mathbf{M}_2(\mathbf{A}) \cdot \mathbf{F} + O(\mathrm{De}^2), \tag{42}$$

where the two mobility tensors $\mathbf{M}_1$ and $\mathbf{M}_2$ are given by

$$\mathbf{M}_1(\mathbf{A}) = \mathbf{I} + \frac{\Psi_1}{35\eta_0}(\mathbf{A} + \mathbf{A}^T), \tag{43}$$

$$\mathbf{M}_2(\mathbf{A}) = M_0 \left\{ \mathbf{I} + \frac{\Psi_1}{\eta_0} \left[f_1(\lambda)\mathbf{A} + f_2(\lambda)\mathbf{A}^T \right] \right\}, \tag{44}$$

with $M_0 = 1/6\pi\eta_0 a$. A result similar to Eq. (42) had previously been obtained by Brunn,[41] though we are unable to match the coefficients in our solution to his. An important consequence of Eq. (44) is that depending on the nature of the local velocity gradient $\mathbf{A} = \nabla\mathbf{V}$ the settling velocity of the sphere may have non-zero components in directions perpendicular to gravity.

C. Direction of motion and physical interpretation

In a vertical shear flow of the form $\mathbf{u}(\mathbf{x}) = -\dot{\gamma}x\hat{\mathbf{z}}$ (such as the one depicted in Fig. 1), for which $\mathbf{V}_0 = \mathbf{0}$ and $\mathbf{A} = -\dot{\gamma}\hat{\mathbf{x}}\hat{\mathbf{z}}$, we find that the settling velocity of the sphere under the gravitational force $\mathbf{F} = -F\hat{\mathbf{z}}$ is given by

$$\mathbf{U}_p = -M_0 F\hat{\mathbf{z}} + [M_0\Psi_1 f_1(\lambda)\dot{\gamma}F/\eta_0]\hat{\mathbf{x}} + O(\mathrm{De}^2). \tag{45}$$

Noting that $\Psi_1 \geq 0$ and $f_1(\lambda) \geq 0$ (since $\lambda \geq 0$ for polymeric solutions and melts[42]), the horizontal component of the settling velocity $\mathbf{U}_p$ is therefore directed toward the half-space where $\mathbf{F} \cdot \mathbf{u}(\mathbf{x}) > 0$, i.e., toward the right in Fig. 1.

The origin of this horizontal drift velocity can be easily understood physically: in the situation of Fig. 1, the left side of the sphere, where the external fluid velocity and the gravitational force point in opposite directions, effectively experiences a stronger shear rate than the right side of the sphere, where fluid velocity and gravity point in the same direction. Combined with the curvature of the surface, this effect results in a net imbalance of normal stresses between the two sides of the sphere, which causes it to migrate toward the right. As we proceed to show next, this non-zero horizontal velocity is responsible for a concentration instability in homogeneous suspensions.
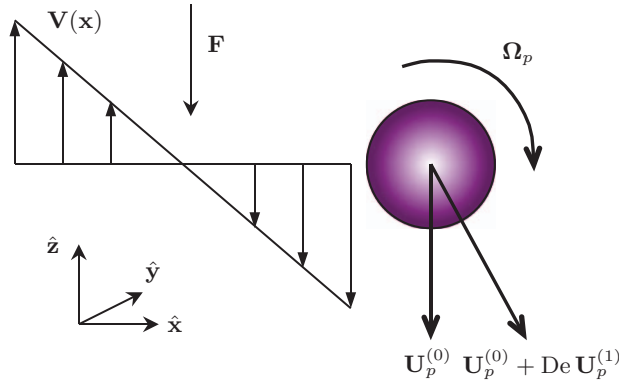
FIG. 1. Sedimentation of an isolated sphere in a linear flow of a second-order fluid.

D. Stability of a homogeneous suspension under sedimentation

We now turn our focus on the stability of a large-scale dilute homogeneous suspension of sedimenting spheres in a second-order fluid, and develop a continuum theory to understand the effect of the drift velocity described above on suspension stability. We adopt an approach similar to that proposed by Koch and Shaqfeh[26] and Saintillan *et al.*[32,33] for spheroids and for deformable particles, and represent the configuration of the suspension by a continuous variable $c(\mathbf{x}, t)$ denoting the concentration of particles at position $\mathbf{x}$ and time t inside the suspension. This variable is normalized as

$$\frac{1}{V} \int_V c(\mathbf{x}, t) \, dV = n, \tag{46}$$

where V is the volume of the container and n is the mean number density of particles in the suspension. Its evolution is governed by a conservation equation:

$$\frac{\partial c}{\partial t} + \nabla \cdot (\dot{\mathbf{x}} c) = 0, \tag{47}$$

in which the flux velocity $\dot{\mathbf{x}}$ can be modeled in dimensional variables as

$$\dot{\mathbf{x}} = \mathbf{M}_1[\nabla \mathbf{u}(\mathbf{x})] \cdot \mathbf{u}(\mathbf{x}) + \mathbf{M}_2[\nabla \mathbf{u}(\mathbf{x})] \cdot \mathbf{F} - \mathbf{D} \cdot \nabla \ln c(\mathbf{x}). \tag{48}$$

In particular, $\dot{\mathbf{x}}$ is written as the sum of the velocity of a particle placed in the local flow field $\mathbf{u}(\mathbf{x})$ induced by the remaining particles in the suspension, of the settling velocity of that particle in the velocity gradient $\nabla \mathbf{u}(\mathbf{x})$, and of a diffusive term (with diffusion tensor $\mathbf{D}$ assumed constant), which may represent the effects of Brownian motion in the case of a colloidal suspension, or of hydrodynamic diffusion. The use of Eqs. (43) and (44) for the particle velocities is contingent upon an assumption of weak viscoelasticity, and the error in Eq. (48) is $O(\mathrm{De}^2)$.

To close Eqs. (47) and (48), the fluid velocity field $\mathbf{u}(\mathbf{x})$ must be determined. It satisfies the continuity equation $\nabla \cdot \mathbf{u} = 0$, together with the following momentum equation, in which we include a forcing term corresponding to the weight exerted by the particles on the fluid:

$$-\eta_0 \nabla^2 \mathbf{u} + \nabla p = \nabla \cdot \mathbf{\Sigma}(\mathbf{u}) + \mathbf{F}[c(\mathbf{x}) - n]. \tag{49}$$

In the following analysis, we assume that the concentration fluctuations are small, i.e., that $c(\mathbf{x}, t) - n = \epsilon c'(\mathbf{x}, t)$ with $|\epsilon| \ll 1$ and $c'(\mathbf{x}, t) = O(n)$.

First, we argue that for the purpose of determining the flux velocity $\dot{\mathbf{x}}$ the nonlinear term in the momentum equation can be neglected to leading order. Indeed, in the limit of weak viscoelasticity, the solution of Eq. (49) may once again be written as a regular expansion $\mathbf{u}(\mathbf{x}) \approx \mathbf{u}^{(0)}(\mathbf{x}) + \mathbf{u}^{(1)}(\mathbf{x}) + \cdots$ where $\mathbf{u}^{(0)}$ is the Newtonian solution, $\mathbf{u}^{(1)}$ is the first correction due to viscoelasticity which is $O(\mathrm{De})$, etc. If we assume that the concentration fluctuations in the suspension occur over a length scale L (typically, the container width), the following scales U_0 and U_1 for $\mathbf{u}^{(0)}$ and $\mathbf{u}^{(1)}$ may be obtained by inspection of Eq. (49): $U_0 = \epsilon F n L^2/\eta_0$ and $U_1 = \mathrm{De}\, U_0$, where $\mathrm{De} = \Psi_1 U_0/\eta_0 L$. The scale U_1

should be compared to the scale for the viscoelastic correction in the settling velocity in Eq. (48), which is De $F/\eta_0 a$. The nonlinear terms in Eq. (49), of magnitude De U_0 and smaller, may therefore be neglected if $U_0 \ll F/\eta_0 a$, which can be shown to be equivalent to $\epsilon \ll (1/\phi_0) \times (a/L)^2$, where ϕ_0 is the mean suspension volume fraction, related to the number density by $\phi_0 = (4\pi a^3/3)n$. In a typical sedimentation experiment (e.g., Bergougnoux et al.[8]), $\phi_0 \sim 10^{-3}$, $a \sim 1$ mm, and $L \sim 10$ cm, which yields $\epsilon \ll 10^{-1}$. For concentration fluctuations that satisfy this condition, the momentum equation (49) may therefore be replaced by

$$- \eta_0 \nabla^2 \mathbf{u} + \nabla p = \mathbf{F}[c(\mathbf{x}) - n], \tag{50}$$

which will result in an $O(\epsilon \text{De})$ error in the calculation of the flux velocity in Eq. (48).

We are now ready to perform the linear stability analysis. We take the base state of the suspension to be uniform in space: $c(\mathbf{x}, t) = n$. In this case, the solution of the flow problem is easily shown to be: $\mathbf{u}(\mathbf{x}) = \mathbf{0}$, and $p = p_0$. To investigate the stability, we consider a weak perturbation with respect to this base state:

$$c(\mathbf{x}, t) = n + \epsilon c'(\mathbf{x}, t). \tag{51}$$

This perturbation induces a weak disturbance flow $\mathbf{u}(\mathbf{x}) = \epsilon \mathbf{u}'(\mathbf{x})$, and pressure perturbation $p = p_0 + \epsilon p'$. Substituting the expressions for c and $\mathbf{u}$ into Eqs. (47) and (48) and neglecting terms of $O(\epsilon^2)$ yields the following linearized equation for $c'(\mathbf{x}, t)$:

$$\frac{\partial c'}{\partial t} + M_0 \mathbf{F} \cdot \nabla c' + \frac{M_0 n \Psi_1}{\eta_0} \nabla \cdot [(f_1(\lambda)\nabla \mathbf{u}' + f_2(\lambda)\nabla \mathbf{u}'^T) \cdot \mathbf{F}] - \nabla \cdot (\mathbf{D} \cdot \nabla c') = 0. \tag{52}$$

Assume a normal mode perturbation with wavevector $\mathbf{k}$: $c'(\mathbf{x}, t) = \tilde{c}(\mathbf{k}) \exp(i\mathbf{k} \cdot \mathbf{x} + \sigma t)$. The corresponding velocity perturbation may also be written $\mathbf{u}'(\mathbf{x}) = \tilde{\mathbf{u}}(\mathbf{k}) \exp(i\mathbf{k} \cdot \mathbf{x} + \sigma t)$, where the Fourier coefficient $\tilde{\mathbf{u}}(\mathbf{k})$ can be obtained by Fourier transform of the momentum equation (50) and by application of the pressure projection operator:[46]

$$\tilde{\mathbf{u}}(\mathbf{k}) = \frac{1}{\eta_0 k^2} \left(\mathbf{I} - \frac{\mathbf{kk}}{k^2} \right) \cdot \mathbf{F} \tilde{c}(\mathbf{k}). \tag{53}$$

Substituting Eq. (53) into the linearized equation (52) yields:

$$\left[\sigma + iM_0 \mathbf{k} \cdot \mathbf{F} - \frac{M_0 n \Psi_1 f_1(\lambda)}{\eta_0^2} \mathbf{F} \cdot \left(\mathbf{I} - \frac{\mathbf{kk}}{k^2} \right) \cdot \mathbf{F} + \mathbf{k} \cdot \mathbf{D} \cdot \mathbf{k} \right] \tilde{c}(\mathbf{k}) = 0. \tag{54}$$

Denote by Θ the angle formed by the gravitational force $\mathbf{F}$ and the wavevector $\mathbf{k}$, defined by: $\mathbf{F} \cdot \mathbf{k} = Fk \cos \Theta$. Using Eq. (54), the real and imaginary parts of σ are readily obtained as

$$\sigma_R = \text{Re}(\sigma) = \frac{M_0 n \Psi_1 f_1(\lambda) F^2}{\eta_0^2} \sin^2 \Theta - \mathbf{k} \cdot \mathbf{D} \cdot \mathbf{k}, \tag{55}$$

$$\sigma_I = \text{Im}(\sigma) = -M_0 Fk \cos \Theta. \tag{56}$$

Recalling that $\Psi_1 \geq 0$ and $f_1(\lambda) \geq 0$, we find that the growth rate σ_R for the concentration fluctuations is positive at low wavenumbers (or long scales) for wavevectors $\mathbf{k}$ that have a non-zero component in a direction perpendicular to gravity ($\sin \Theta \neq 0$), and is maximum when $\Theta = \pi/2$, corresponding to horizontal density waves. At high wavenumbers, particle diffusion damps this growth rate and stabilizes the suspension. The growth rate is plotted as a function of the wavenumber for various wave angles in Fig. 2(a), in which the following dimensionless variables are used:

$$\sigma_R^* = \frac{\eta_0^2 \sigma_R}{M_0 n \Psi_1 f_1(\lambda) F^2}, \quad \mathbf{k}^* = \frac{\mathbf{k}}{n^{1/3}}, \quad \mathbf{D}^* = \frac{\eta_0^2 \mathbf{D}}{M_0 n^{1/3} \Psi_1 f_1(\lambda) F^2}. \tag{57}$$

The mechanism for the instability is illustrated in Fig. 2(b) and is qualitatively similar to that described by Koch and Shaqfeh[26] for spheroids and by Saintillan et al.[32] for deformable particles in Newtonian fluids. Specifically, a weak concentration fluctuation in the suspension (e.g., due to the initial random mixing) will create a disturbance flow, which points downwards in the high-density regions and upwards in the low-density regions. When a sphere sediments in this flow, the
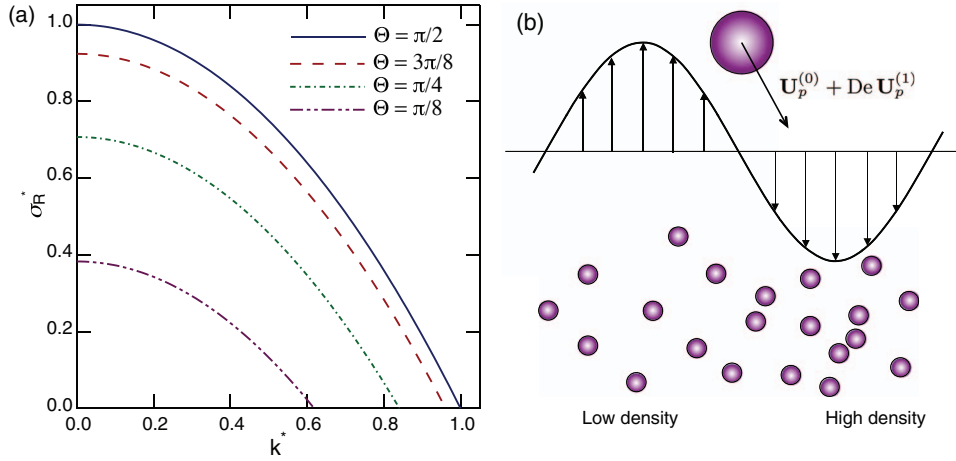
FIG. 2. (a) Dimensionless growth rate σ_R^* as a function of the wavenumber k^* for various wave angles Θ. In this plot, the dimensionless diffusion tensor was taken to be the identity tensor: $\mathbf{D}^* = \mathbf{I}$. (b) Mechanism for the instability: a weak concentration fluctuation creates a disturbance flow which causes the particles to settle preferentially toward the denser regions (after Koch and Shaqfeh[26]).

nonlinear coupling of its settling motion with the local flow field owing to viscoelastic effects causes it to migrate toward the denser regions, according to the discussion of Sec. II C. This migration has the effect of reinforcing the initial concentration fluctuation, thereby leading to the growth of inhomogeneities. Based on this analysis, we expect large-scale density fluctuations to grow with time, with the longest wavelengths growing fastest: in a bounded system, the strongest inhomogeneities are therefore expected to occur on the scale of the container, at least in the linear regime.

The mechanism described here is similar to that previously proposed by Phillips.[39] Phillips started from pair particle interactions in a second-order fluid (calculated asymptotically in the limit of weak viscoelasticity and widely separated particles[24]), and integrated these interactions over a uniform particle distribution perturbed by a sine wave in a horizontal direction. After averaging, he obtains a horizontal particle flux that causes particles to migrate preferentially toward dense regions. In the mechanism proposed herein, we consider the mean-field flow field generated by an arbitrary distribution of particles on the scale of the suspension, and analyze the migration of a test particle in this flow field as a result of non-Newtonian effects. Note that in addition to this mean-field effect, pair particle interactions may also play a role at shorter length scales and cause local particle aggregation and chaining, as previously studied by Phillips and Talini;[24] such local interactions are not easily included in the continuum framework of the present model.

The influence of the normal stress coefficients is clear from expressions such as Eqs. (45) and (55), where the growth rate for long-wavelength perturbations, which is directly related to the horizontal drift velocity, is proportional to $\Psi_1 f_1(\lambda) = 5\Psi_1/64 - \Psi_2/2$. Since $\Psi_2 < 0$ for polymeric fluids, both normal stress coefficients have a destabilizing effect, which is consistent with the previous finding of Phillips.[39] For a given value of Ψ_1, the growth rate is minimum when $\Psi_2 = 0$ (or $\lambda = 0$), corresponding to the case of a Weissenberg fluid.

III. NUMERICAL SIMULATIONS

The linear stability analysis of Sec. II D provides a mechanism for the growth of concentration fluctuations in the suspensions, but is limited to a weak initial density fluctuation satisfying $\epsilon \ll (1/\phi_0) \times (a/L)^2$. This very stringent condition is unlikely to be met in most sedimentation experiments, where even well-mixed suspensions have significant random number density fluctuations. In addition, the analysis only captures the linear regime and does not account for finite system sizes. To confirm the results of the linear analysis but also investigate the effects of nonlinearities, finite system size, and random initial distributions, we also perform direct numerical simulations of

dilute particle suspensions using a point-particle model and a weakly nonlinear approach, which we proceed to describe here.

A. Simulation method

1. Governing equations

The method of simulation is an extension of the previous work of Bergougnoux et al.[8] and Saintillan et al.[32] for Newtonian fluids, which is based on a point-particle model and a spectral solution of the Stokes equations. We consider a suspension of M identical spheres of radius a suspended in a container of dimensions $L_x \times L_y \times L_z$ filled with a second-order fluid, where the gravitational force on the particles points in the negative z-direction: $\mathbf{F} = -F\hat{\mathbf{z}}$. The suspension is assumed to be dilute, i.e., the mean interparticle distance $n^{-1/3}$ (where n is the mean number density) is assumed to be much greater than the particle radius. Denoting by $\mathbf{x}_\alpha$ the center-of-mass position of particle α (for $\alpha = 1, \ldots, M$), the translational velocity $\dot{\mathbf{x}}_\alpha$ of a particle is obtained to order $O(\mathrm{De})$ by application of the mobility relation Eq. (42) derived in Sec. II B:

$$\dot{\mathbf{x}}_\alpha = \mathbf{M}_1[\nabla\mathbf{u}(\mathbf{x}_\alpha)] \cdot \mathbf{u}(\mathbf{x}_\alpha) + \mathbf{M}_2[\nabla\mathbf{u}(\mathbf{x}_\alpha)] \cdot \mathbf{F} + O(\mathrm{De}^2). \tag{58}$$

Here, $\mathbf{u}(\mathbf{x})$ denotes the velocity field driven by the particles as they sediment through the fluid, and satisfies the continuity and momentum equations:

$$\nabla \cdot \mathbf{u} = 0, \quad -\eta_0\nabla^2\mathbf{u} + \nabla p = \nabla \cdot \mathbf{\Sigma}(\mathbf{u}) + \mathbf{f}(\mathbf{x}). \tag{59}$$

In the momentum equation, the force distribution $\mathbf{f}(\mathbf{x})$ corresponds to the forces exerted by the particles on the fluid. In the case of identical point particles subject to a gravitational force $\mathbf{F}$, it is obtained as

$$\mathbf{f}(\mathbf{x}) = \mathbf{F} \sum_{\beta=1}^{M} \delta(\mathbf{x} - \mathbf{x}_\beta), \tag{60}$$

where δ denotes the three-dimensional Dirac delta function. Equations (58)–(60) form a closed system of equations which can be solved by time-marching of the particle positions, and requires a solution of Eq. (59) at each time step.

2. Mean-field flow solution

The numerical solution of Eqs. (59) and (60) proceeds as follows. Knowing the particle positions from the previous time step (or from the initial configuration), the force distribution $\mathbf{f}(\mathbf{x})$ is calculated on a Cartesian grid (with $K_x \times K_y \times K_z$ grid points) by linear interpolation. The number of grid points is chosen so that the mesh size is smaller than the mean interparticle distance. Once the force distribution is known on the grid, the nonlinear momentum equation is solved iteratively to $O(\mathrm{De})$, for consistency with the order of approximation of the mobility relation Eq. (58). Specifically, we first solve for the Newtonian solution $(\mathbf{u}^{(0)}, p^{(0)})$ (using a spectral method described below), which satisfies the linear Stokes equations

$$\nabla \cdot \mathbf{u}^{(0)} = 0, \quad -\eta_0\nabla^2\mathbf{u}^{(0)} + \nabla p^{(0)} = \mathbf{f}(\mathbf{x}). \tag{61}$$

After the Newtonian $O(\mathrm{De}^0)$ solution is obtained, it is used to calculate the non-Newtonian stress on the right-hand side of Eq. (59). As a second step to the iterative method, we then solve the problem

$$\nabla \cdot \mathbf{u} = 0, \quad -\eta_0\nabla^2\mathbf{u} + \nabla p = \nabla \cdot \mathbf{\Sigma}(\mathbf{u}^{(0)}) + \mathbf{f}(\mathbf{x}), \tag{62}$$

which yields a solution to Eq. (59) accurate to $O(\mathrm{De})$. One significant advantage of this iterative process is that the right-hand side in Eq. (62) is known, and therefore the equations are linear and can be solved using standard methods for Stokes flow. Once the velocity field $\mathbf{u}(\mathbf{x})$ is known, it is differentiated on the grid by second-order central finite differences to obtain $\nabla\mathbf{u}(\mathbf{x})$. The values of the velocity and velocity gradient at the particle locations, which are required in Eq. (58), are

then obtained by interpolation from the grid values; in the simulations described below, third-order B-splines are used for interpolation.[47]

For both steps of the iterative method, the Stokes equations need to be solved on the grid, with a known force density $\mathbf{g}(\mathbf{x})$, representing either $\mathbf{f}(\mathbf{x})$ or $[\nabla \cdot \mathbf{\Sigma}(\mathbf{u}^{(0)}) + \mathbf{f}(\mathbf{x})]$. The following boundary conditions are enforced at the container walls:

$$\mathbf{n} \cdot \mathbf{u}(\mathbf{x}) = 0, \quad \mathbf{n} \cdot \nabla[(\mathbf{l} - \mathbf{nn}) \cdot \mathbf{u}(\mathbf{x})] = \mathbf{0}, \tag{63}$$

where $\mathbf{n}$ is a unit vector normal to the boundary. The first condition enforces no fluid penetration, whereas the second one corresponds to a free-shear-stress boundary condition. While this differs from the no-slip boundary condition applying at the walls of a rigid container, it has the advantage of allowing for a very efficient spectral solution while preventing fluid penetration at the boundaries, a feature that has previously been shown to be critical in sedimentation simulations.[7] Previous simulations of sphere suspensions,[8, 12, 48] as well as spheroid suspensions,[32, 33] have demonstrated that this boundary condition is sufficient to capture most salient features observed in sedimentation experiments, including the decay of velocity fluctuations in sphere suspensions,[12] and a wavenumber selection for density fluctuations in spheroid suspensions.[33] Note, however, that owing to the free-shear-stress condition there is no resistance to tangential flow close the the boundaries, which may have a quantitative effect on velocity fluctuations in the suspensions.

The spectral solution of the Stokes equations is obtained as follows. We first decompose the force density $\mathbf{g}(\mathbf{x})$ as the sum of its three components in the x, y, and z directions:

$$\mathbf{g}(\mathbf{x}) = g_1(\mathbf{x})\hat{\mathbf{x}} + g_2(\mathbf{x})\hat{\mathbf{y}} + g_3(\mathbf{x})\hat{\mathbf{z}}. \tag{64}$$

By linearity of the Stokes equations, it is possible to solve three independent problems for the three functions g_1, g_2, and g_3, with solutions $\mathbf{u}_1(\mathbf{x})$, $\mathbf{u}_2(\mathbf{x})$, and $\mathbf{u}_3(\mathbf{x})$. The full flow velocity $\mathbf{u}(\mathbf{x})$ driven by the force density $\mathbf{g}(\mathbf{x})$ is then obtained by superposition. The solution of the first problem (for $\mathbf{u}_1$) proceeds as follows. In order to satisfy the boundary conditions of Eq. (63), we seek a solution in terms of truncated sine and cosine series:[8, 32]

$$\mathbf{u}_1(\mathbf{x}) = \sum_{\mathbf{k}} \left\{ \begin{array}{l} \widetilde{u}_{1x}(\mathbf{k}) \sin\left(\dfrac{\pi k_x x}{L_x}\right) \cos\left(\dfrac{\pi k_y y}{L_y}\right) \cos\left(\dfrac{\pi k_z z}{L_z}\right) \\[2ex] \widetilde{u}_{1y}(\mathbf{k}) \cos\left(\dfrac{\pi k_x x}{L_x}\right) \sin\left(\dfrac{\pi k_y y}{L_y}\right) \cos\left(\dfrac{\pi k_z z}{L_z}\right) \\[2ex] \widetilde{u}_{1z}(\mathbf{k}) \cos\left(\dfrac{\pi k_x x}{L_x}\right) \cos\left(\dfrac{\pi k_y y}{L_y}\right) \sin\left(\dfrac{\pi k_z z}{L_z}\right) \end{array} \right\}, \tag{65}$$

where the wavevector $\mathbf{k}$ is defined as

$$\mathbf{k} = \frac{k_x}{L_x}\hat{\mathbf{x}} + \frac{k_y}{L_y}\hat{\mathbf{y}} + \frac{k_y}{L_y}\hat{\mathbf{y}} \tag{66}$$

with $k_x = 1, \ldots, K_x$, $k_y = 1, \ldots, K_y$, and $k_z = 1, \ldots, K_z$. This choice of sine and cosine series in Eq. (65) automatically satisfies the boundary conditions. Substitution of Eq. (65) into the momentum equation then suggests expanding $g_1(\mathbf{x})$ as

$$g_1(\mathbf{x}) = \sum_{\mathbf{k}} \widetilde{g}_1(\mathbf{k}) \sin\left(\frac{\pi k_x x}{L_x}\right) \cos\left(\frac{\pi k_y y}{L_y}\right) \cos\left(\frac{\pi k_z z}{L_z}\right). \tag{67}$$

After elementary manipulations, it is possible to show that the momentum and continuity equations for $\mathbf{u}_1$ are exactly satisfied provided that

$$\widetilde{u}_{1x}(\mathbf{k}) = -\left(\frac{k_y^2}{L_y^2} + \frac{k_z^2}{L_z^2}\right)\widetilde{u}_1(\mathbf{k}), \quad \widetilde{u}_{1y}(\mathbf{k}) = \frac{k_x k_y}{L_x L_y}\widetilde{u}_1(\mathbf{k}), \quad \widetilde{u}_{1z}(\mathbf{k}) = \frac{k_x k_z}{L_x L_z}\widetilde{u}_1(\mathbf{k}), \tag{68}$$

where the coefficient $\widetilde{u}_1(\mathbf{k})$ is given by

$$\widetilde{u}_1(\mathbf{k}) = -\frac{\widetilde{g}_1(\mathbf{k})}{\eta_0 \pi^2 \left[\left(\frac{k_x}{L_x}\right)^2 + \left(\frac{k_y}{L_y}\right)^2 + \left(\frac{k_z}{L_z}\right)^2\right]^2}. \tag{69}$$

In the simulations, fast sine and cosine transform algorithms are used to calculate $\widetilde{g}_1(\mathbf{k})$ in Eq. (67), from which the velocity field is obtained by application of Eqs. (65), (68) and (69). The two additional flow fields $\mathbf{u}_2(\mathbf{x})$ and $\mathbf{u}_3(\mathbf{x})$ corresponding to the other two components of force are obtained by straightforward modifications of Eqs. (65) and (67).

In the following discussion, we non-dimensionalize all the variables using the length scale a (radius of a particle), velocity scale $U_s = F/6\pi \eta_0 a$ (Stokes velocity in the Newtonian solvent), and corresponding time scale a/U_s. All simulations are performed in a box of dimensions $L_x \times L_y \times L_z = 300 \times 300 \times 1200$, and the number of grid points (or Fourier modes) is chosen to be $65 \times 65 \times 257$. We use a dilute volume fraction of $\phi_0 = 0.5\,\%$, corresponding to a total of 128 915 particles in the simulation domain. The ratio $\lambda = -4\Psi_2/\Psi_1$ of the normal stress coefficients is set to 2, and we vary the value of the Deborah number De $= \Psi_1 U_s/\eta_0 a$ from 0 to 1 to investigate the effects of viscoelasticity. Note that the simulation method described here is only valid for weak viscoelasticity (De $\ll$ 1), so the results for De $= 1$ are unlikely to be quantitatively accurate; yet, we do not expect the dynamics to change qualitatively over the range of Deborah numbers considered here.

B. Results and discussion

The evolution of the concentration field in two typical simulations at De $= 0$ and 1 is illustrated in Fig. 3. In the absence of viscoelasticity [De $= 0$, Fig. 3(a)], significant density fluctuations exist owing to the initial random distribution of the particles, which follows a Poisson distribution. These fluctuations are also observed in experiments, where they may follow statistics that depart slightly
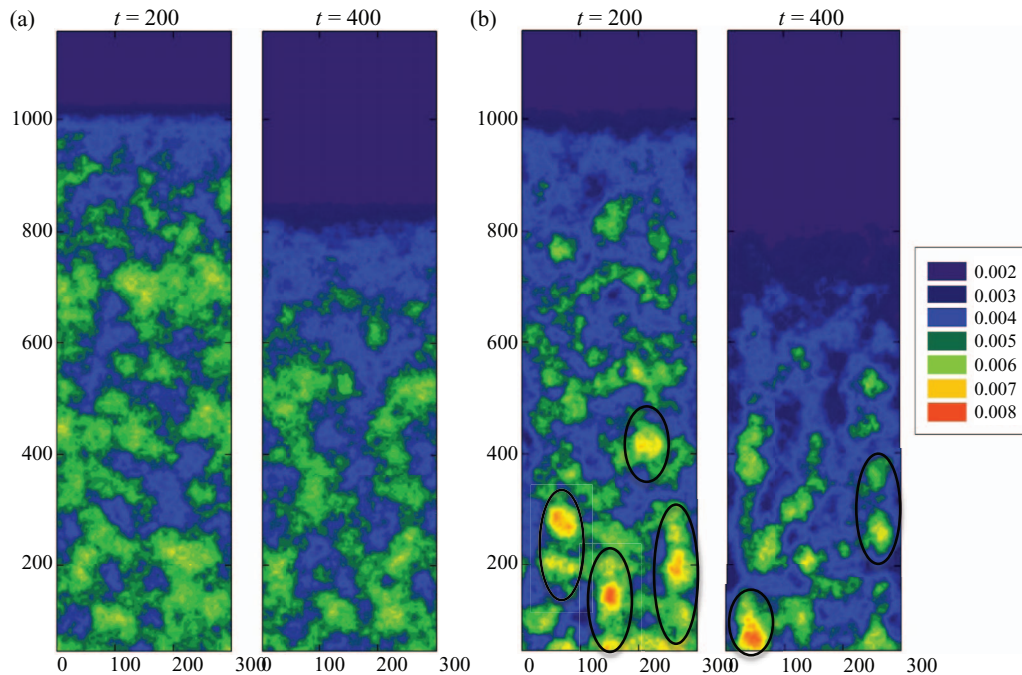

FIG. 3. Concentration field, inferred from particle positions, at two different instants, in simulations of 128 915 spheres sedimenting in a container of dimensions $300 \times 300 \times 1200$ (mean volume fraction $\phi_0 = 0.5\,\%$): (a) De $= 0.0$ (Newtonian), and (b) De $= 1.0$ (viscoelastic). In the viscoelastic case, dense vertical clusters are observed to form, as highlighted by the black closed contours.
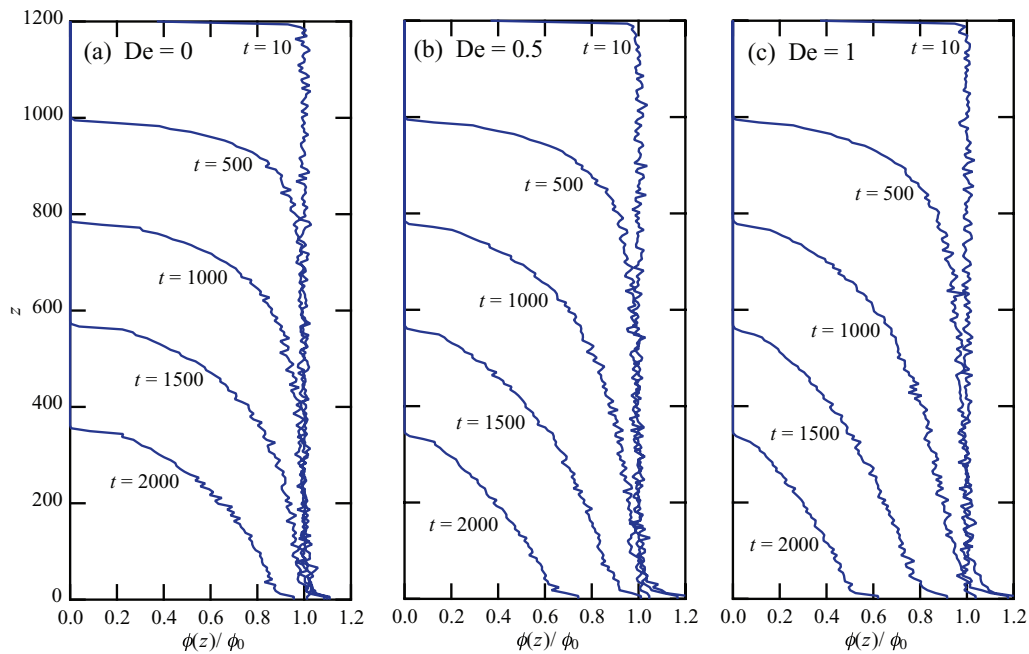
FIG. 4. Vertical density profiles at various times in simulations of 128 915 spheres sedimenting in a container of dimensions $300 \times 300 \times 1200$ (mean volume fraction $\phi_0 = 0.5\,\%$): (a) De = 0.0, (b) De = 0.5, and (c) De = 1.0. The figure shows averages over 10 simulations with distinct initial conditions.

from Poisson[13] but are comparable in magnitude. One key feature to be noted is that the magnitude of these fluctuations remains sensibly the same with time, as will be confirmed more quantitatively below. However, in the case of a viscoelastic fluid (De = 1), much stronger concentration fluctuations are observed, as demonstrated in Fig. 3(b) by dense spots (highlighted by black closed contours) surrounded by clarified regions. The growth of density fluctuations, which is in qualitative agreement with experimental observations,[21] supports our prediction of Sec. II D of a concentration instability. In the simulations, we find that fluctuations become stronger as the Deborah number is increased. We also find that they tend to grow over time (at least initially, as their growth eventually competes with hydrodynamic diffusion and the developing stratification also tends to damp the dynamics), and a qualitative observation of the concentration field at late times [e.g., $t = 400$ in Fig. 3(b)] suggests that a structuring of the suspension is taking place in the form of dense vertical columns or streamers separated by relatively clear fluid. This structuring, which is reminiscent of the streamer formation in settling suspensions of rodlike particles,[30,32–34] was also reported in experiments in non-Newtonian fluids[21] and hints at a wavenumber selection not predicted by the simple linear analysis of Sec. II D.

Another feature visible in Fig. 3 is the development of a broad suspension front, as a result of the rapid settling of the dense clusters and streamers out of suspension. This is shown more precisely in Fig. 4, where we plot vertical concentration profiles at various times for three values of the Deborah number. In the Newtonian case [Fig. 4(a)], a diffuse concentration front is found to develop and spread at the interface with the clear fluid, as previously characterized in experiments and simulations;[8,12,48] however, the concentration profile remains nearly uniform and equal to the mean concentration in the bulk of the suspension away from the front, except in the late stages of the sedimentation process when the front becomes very broad. In a viscoelastic fluid [Figs. 4(b) and 4(c)], the suspension front is observed to spread more rapidly, and vertical density gradients are seen to form in the bulk away from the front. This strong stratification, which is not observed at De = 0, is easily understood as a consequence of the formation of dense clusters, which sediment rapidly out of suspension and leave clarified fluid in their wake. Similar observations had previously been made on the sedimentation of anisotropic particles in a Newtonian fluid.[32,33] In that case, it has
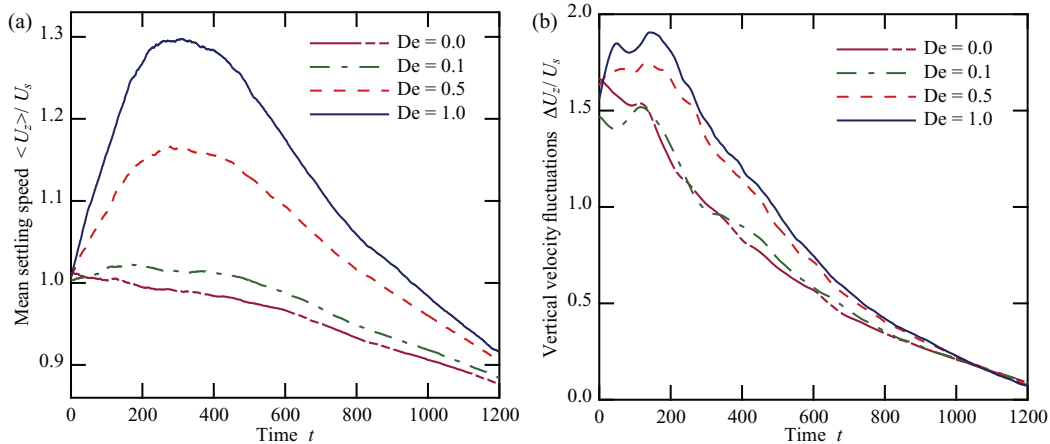
FIG. 5. (a) Mean settling velocity $\langle U_z \rangle / U_s$ and (b) standard deviation $\Delta U_z / U_s$ of the vertical velocity as functions of time at various Deborah numbers. The figure shows averages over 10 simulations with distinct initial conditions.

previously been argued that stratification may play a role in the structuring of the density fluctuations in the form of vertical streamers by setting a critical length scale beyond which fluctuations cannot grow.[33] While this mechanism is still debated and not fully supported by experiments,[49] it may be at play in the instability of spherical particles in viscoelastic fluids as well, and may explain the formation of vertical columns observed in Fig. 3(b). Additional work is needed to elucidate this effect.

In addition to stratification, the clustering of the particles as a result of the instability also leads to an enhancement of the mean settling speed and velocity fluctuations. Both quantities are plotted as functions of time for different values of the Deborah number in Fig. 5. When De = 0, the mean settling velocity remains close to the Stokes velocity for an isolated particle, and is even found to decrease slightly with time, an effect that can be attributed to interactions with the bottom boundary when much of the suspension has settled near the bottom of the container. When the Deborah number is non-zero, we observe a significant increase in the mean settling speed as time progresses; this increase is strongest for high values of De, with a peak velocity increase of up to 30 % when De = 1. This enhancement of the settling speed is a direct consequence of the instability, by which dense clusters settle more rapidly than isolated particles. Once most clusters have reached the bottom of the container, the settling velocity starts decreasing again to reach values close to the Stokes velocity in the later stages of the sedimentation process. Similar trends are observed on the velocity fluctuations in Fig. 5(b): the clustering instability in the viscoelastic case causes an increase in the standard deviation of the vertical velocity, a consequence of the significant difference in settling speed between particles captured inside clusters and particles suspended in clarified regions. Regardless of the value of the Deborah number, we find, however, that the velocity fluctuations are rapidly damped in the suspensions, a likely consequence of the small system sizes used in the simulations and of the developing stratification observed on Fig. 4.

The density fluctuations resulting from the concentration instability can be characterized more quantitatively by considering the evolution of particle occupancy statistics in the suspensions.[5,13] Given a small cubic interrogation cell of volume V placed inside the suspension, the mean number of particles inside the cell is expected to be $\langle N \rangle = \phi_0 V / V_p$, where $V_p = 4\pi a^3 / 3$ is the volume of a particle. When such a cell is placed at an arbitrary location in the suspension, it contains a number N of particles that will in general differ from the expected value of $\langle N \rangle$ owing to fluctuations, and follows a distribution $P(N)$. In a perfectly random suspension following Poisson statistics, this distribution is given by $P(N) = \langle N \rangle^N \exp(-\langle N \rangle)/N!$, with a standard deviation of $\sigma_N = \langle N \rangle^{1/2}$. Departures from this law are indicative of the level of number density fluctuations on the scale of the interrogation cell. Distributions $P(N)$, for $\langle N \rangle = 10$, are shown at different times in Figs. 6(a)
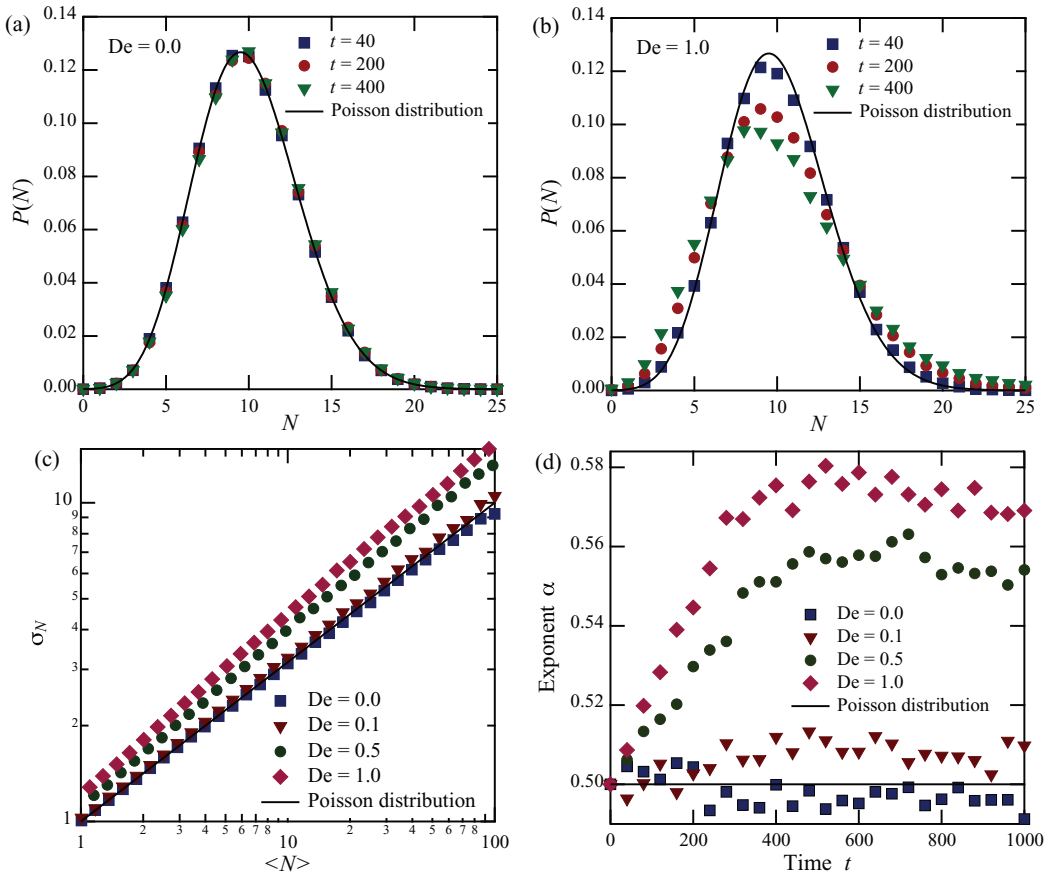
FIG. 6. (a)–(b) Particle occupancy distributions $P(N)$ for $\langle N \rangle = 10$ at various times t at two different Deborah numbers: (a) De $= 0$ (Newtonian), and (b) De $= 1$ (viscoelastic). The distributions are compared to the Poisson distribution $P(N) = \langle N \rangle^N \exp(-\langle N \rangle)/N!$ (c) Standard deviation σ_N of $P(N)$ versus $\langle N \rangle$ at $t = 400$. The standard deviation exhibits a power-law dependence $\sigma \sim \langle N \rangle^\alpha$, with an exponent of 1/2 for a random suspension with Poisson statistics. (d) Evolution of the exponent α as a function of time for various Deborah numbers.

and 6(b) in the Newtonian and viscoelastic cases, and are compared to the Poisson distribution. When De $= 0$ [Fig. 6(a)], the particle occupancy distributions agree very well with the Poisson distribution at all times, and do not significantly evolve during sedimentation. Such is not the case for De $= 1.0$, where we see that the distributions are close to the Poisson distribution early on (indeed, the initial distribution is chosen to be perfectly random), but tend to become broader and flatter as sedimentation takes place. These giant number fluctuations indicate that a large number of interrogation cells contain either too many or too few particles (compared to a random distribution), which is consistent with the local clustering of the particles discussed above.

The effect of scale is analyzed in Fig. 6(c), where the standard deviation σ_N of the distributions is plotted versus the mean $\langle N \rangle$ at $t = 400$. A power-law dependence $\sigma_N \sim \langle N \rangle^\alpha$ is observed in all cases. In the Newtonian case, the exponent is found to be very close to 1/2 as expected for a random suspension with Poisson statistics. The exponent α is, however, found to increase with Deborah number when viscoelasticity is present. This is further confirmed in Fig. 6(d), showing the evolution of α with time at different Deborah numbers. Only a weak evolution is observed in the Newtonian case: we indeed see that α decreases slightly below the value of 1/2, which corresponds to a suppression of fluctuations during sedimentation, an effect previously reported in other simulations as well.[7] However, α increases with time in viscoelastic suspensions as clusters form and grow, and reaches a statistical steady state at a value that depends on the Deborah number and can be as high as ≈ 0.57 for De $= 1$.

IV. CONCLUDING REMARKS

Using a linear stability analysis, we have shown that a suspension of spherical particles sedimenting under gravity in a viscoelastic fluid is unstable to concentration fluctuations. This instability, which shares strong similarities with other concentration instabilities occurring in sedimenting suspensions of anisotropic or deformable particles in Newtonian fluids,[26, 32] results from the nonlinear coupling between the mobility of a sphere and the local flow field around the particle driven by the density fluctuations in the suspension through hydrodynamic interactions. While the present analysis is specifically concerned with a second-order fluid, we anticipate that qualitatively similar results may hold for other types of viscoelastic fluids too, as the only requirement for the coupling between mobility and local flow is a nonlinear constitutive relation. The instability described herein is consistent with and may explain the recent experimental findings of Mora *et al.*,[21] who observed the formation of inhomogeneities in sedimenting suspensions in polymeric solutions.

To further analyze the long-time evolution of the suspensions in the nonlinear regime, as well as investigate the effects of finite system sizes and random initial distributions, we also developed a simple simulation method based on a point-particle approximation and on a weakly nonlinear solution of the momentum equation for the mean-field fluid velocity in the suspension. These simulations confirmed the existence of an instability, which manifests itself in the form of dense cluster separated by clarified fluid. Our simulations suggest that these clusters tend to organize in vertical columns and that a horizontal wavenumber selection not predicted by the linear analysis may be taking place. While further work is needed to fully characterize this effect, a possible mechanism for such a wavenumber selection is the strong stratification that was found to develop in the suspensions.[33] The instability was also found to result in a significant enhancement of the mean settling speed (by up to 30 % for De = 1.0) and of velocity fluctuations. Both effects are again easily understood as consequences of the clustering.

It should be noted that both the theory and simulations described herein are valid only for a second-order fluid in the limit of weak viscoelasticity (small Deborah number), a case amenable to asymptotic solutions and perturbation methods. It is unclear whether the concentration instability presented in this work would arise in more complex types of non-Newtonian fluids, where the effects of shear-thinning for instance may introduce qualitatively new dynamics. A detailed analysis for arbitrary Deborah numbers or other constitutive relations may not be amenable to an analytical treatment, and will likely require more sophisticated numerical simulations.

[1] E. Guazzelli and J. Hinch, "Fluctuations and instability in sedimentation," Annu. Rev. Fluid Mech. **43**, 97 (2011).

[2] R. E. Caflisch and J. H. C. Luke, "Variance in the sedimentation speed of a suspension," Phys. Fluids **28**, 759 (1985).

[3] E. J. Hinch, "Sedimentation of small particles," in *Disorder and Mixing*, edited by E. Guyon, J.-P. Nadal, and Y. Pomeau (Kluwer, Dordrecht, 1988).

[4] D. L. Koch and E. S. G. Shaqfeh, "Screening in sedimenting suspensions," J. Fluid Mech. **224**, 275 (1991).

[5] X. Lei, B. J. Ackerson, and P. Tong, "Settling statistics of hard sphere particles," Phys. Rev. Lett. **86**, 3300 (2001).

[6] S.-Y. Tee, P. J. Mucha, L. Cipelletti, S. Manley, M. P. Brenner, P. N. Segre, and D. A. Weitz, "Nonuniversal velocity fluctuations of sedimenting particles," Phys. Rev. Lett. **89**, 054501 (2002).

[7] A. J. C. Ladd, "Effects of container walls on the velocity fluctuations of sedimenting spheres," Phys. Rev. Lett. **88**, 048301 (2002).

[8] L. Bergougnoux, S. Ghicini, E. Guazzelli, and J. Hinch, "Spreading fronts and fluctuations in sedimentation," Phys. Fluids **15**, 1875 (2003).

[9] P. J. Mucha, S.-Y. Tee, D. A. Weitz, B. I. Shraiman, and M. P. Brenner, "A model for velocity fluctuations in sedimentation," J. Fluid Mech. **501**, 71 (2004).

[10] N.-Q. Nguyen and A. J. C. Ladd, "Sedimentation of hard-sphere suspensions at low Reynolds number," J. Fluid Mech. **525**, 73 (2005).

[11] D. Chehata Gómez, L. Bergougnoux, J. Hinch, and E. Guazzelli, "On stratification control of the velocity fluctuations in sedimentation," Phys. Fluids **19**, 098102 (2007).

[12] D. Chehata Gómez, L. Bergougnoux, E. Guazzelli, and J. Hinch, "Fluctuations and stratification in sedimentation of dilute suspensions of spheres," Phys. Fluids **21**, 093304 (2009).

[13] L. Bergougnoux and E. Guazzelli, "Non-Poisson statistics of settling spheres," Phys. Fluids **21**, 091701 (2009).

[14] M. J. Riddle, C. Narvaez, and R. B. Bird, "Interactions between two spheres falling along their line of centers in a viscoelastic fluid," J. Non-Newtonian Fluid Mech. **2**, 23 (1977).

[15] E. Allen and P. H. T. Uhlherr, "Nonhomogeneous sedimentation in viscoelastic fluids," J. Rheol. **33**, 627 (1989).

[16] D. D. Joseph, Y. J. Liu, M. Poletto, and J. Feng, "Aggregation and dispersion of spheres falling in viscoelastic liquids," J. Non-Newtonian Fluid Mech. **54**, 45 (1994).

[17] E. T. G. Bot, M. A. Hulsen, and B. H. A. A. van den Brule, "The motion of two spheres falling along their line of centres in a Boger fluid," J. Non-Newtonian Fluid Mech. **79**, 191 (1998).

[18] S. Bobroff and R. J. Phillips, "Nuclear magnetic resonance imaging investigation of sedimentation of concentrated suspensions in non-Newtonian fluids," J. Rheol. **42**, 1419 (1998).

[19] S. Daugan, L. Talini, B. Herzhaft, and C. Allain, "Aggregation of particles settling in shear-thinning fluids. Part 1. Two-particle aggregation," Eur. Phys. J. E **7**, 73 (2002).

[20] S. Daugan, L. Talini, B. Herzhaft, and C. Allain, "Aggregation of particles settling in shear-thinning fluids. Part 2. Three-particle aggregation," Eur. Phys. J. E **9**, 55 (2002).

[21] S. Mora, L. Talini, and C. Allain, "Structuring sedimentation in a shear-shinning fluid," Phys. Rev. Lett. **95**, 088301 (2005).

[22] M. M. Gumulya, R. R. Horsley, V. Pareek, and D. D. Lichti, "The effects of fluid viscoelasticity on the settling behaviour of horizontally aligned spheres," Chem. Eng. Sci. **66**, 5822 (2011).

[23] Z. Yu, A. Wachs, and Y. Peysson, "Numerical simulations of particle sedimentation in shear-thinning fluids with a fictitious domain method," J. Non-Newtonian Fluid Mech. **136**, 126 (2006).

[24] R. J. Phillips and L. Talini, "Chaining of weakly interacting particles suspended in viscoelastic fluids," J. Non-Newtonian Fluid Mech. **147**, 175 (2007).

[25] E. Verneuil, R. J. Phillips, and L. Talini, "Axisymmetric two-sphere sedimentation in a shear-thinning viscoelastic fluid: Particle interactions and induced fluid velocity fields," J. Rheol. **51**, 1343 (2007).

[26] D. L. Koch and E. S. G. Shaqfeh, "The instability of a dispersion of sedimenting spheroids," J. Fluid Mech. **209**, 521 (1989).

[27] M. B. Mackaplow and E. S. G. Shaqfeh, "A numerical study of the sedimentation of fibre suspensions," J. Fluid Mech. **376**, 149 (1998).

[28] J. E. Butler and E. S. G. Shaqfeh, "Dynamic simulations of the inhomogeneous sedimentation of rigid fibres," J. Fluid Mech. **468**, 205 (2002).

[29] E. Kuusela, J. M. Lahtinen, and T. Ala-Nissila, "Collective effects in settling of spheroids under steady-state sedimentation," Phys. Rev. Lett. **90**, 094502 (2003).

[30] B. Metzger, E. Guazzelli, and J. E. Butler, "Large-scale streamers in the sedimentation of a dilute fiber suspension," Phys. Rev. Lett. **95**, 164506 (2005).

[31] D. Saintillan, E. Darve, and E. S. G. Shaqfeh, "A smooth particle-mesh Ewald algorithm for Stokes suspension simulations: The sedimentation of fibers," Phys. Fluids **17**, 033301 (2005).

[32] D. Saintillan, E. S. G. Shaqfeh, and E. Darve, "The growth of concentration fluctuations in dilute dispersions of orientable and deformable particles under sedimentation," J. Fluid Mech. **553**, 347 (2006).

[33] D. Saintillan, E. S. G. Shaqfeh, and E. Darve, "The effect of stratification on the wave number selection in the instability of sedimenting spheroids," Phys. Fluids **18**, 121503 (2006).

[34] B. Metzger, J. E. Butler, and E. Guazzelli, "Experimental investigation of the instability of a sedimenting suspension of fibers," J. Fluid Mech. **575**, 307 (2007).

[35] K. Gustavsson and A.-K. Tornberg, "Gravity induced sedimentation of slender fibers," Phys. Fluids **21**, 123301 (2009).

[36] M. Manga and H. A. Stone, "Collective hydrodynamics of deformable drops and bubbles in dilute low-Reynolds-number suspensions," J. Fluid Mech. **300**, 231 (1995).

[37] A. Z. Zinchenko and R. H. Davis, "Large-scale simulations of concentrated emulsion flows," Philos. Trans. R. Soc. London, Ser. A **361**, 813 (2003).

[38] V. Narsimhan and E. S. G. Shaqfeh, "Lateral drift and concentration instability in a suspension of bubbles induced by Marangoni stresses at zero Reynolds number," Phys. Fluids **22**, 101702 (2010).

[39] R. J. Phillips, "Structural instability in the sedimentation of particulate suspensions through viscoelastic fluids," J. Non-Newtonian Fluid Mech. **165**, 479 (2010).

[40] R. B. Bird, R. C. Armstrong, and O. Hassager, *Dynamics of Polymeric Liquids* (Wiley-Interscience, Hoboken, 1987).

[41] P. Brunn, "The slow motion of a sphere in a second-order fluid," Rheol. Acta **15**, 163 (1976).

[42] B. P. Ho and L. G. Leal, "Migration of rigid spheres in a two-dimensional unidirectional shear flow of a second-order fluid," J. Fluid Mech. **76**, 783 (1976).

[43] L. G. Leal, "Particle motions in viscous fluids," Annu. Rev. Fluid Mech. **12**, 435 (1980).

[44] S. Kim and S. P. Karrila, *Microhydrodynamics: Principles and Selected Applications* (Butterworth-Heinemann, Oxford, 1991).

[45] J. Happel and H. Brenner, *Low Reynolds Number Hydrodynamics* (Prentice-Hall, Englewood Cliffs, 1965).

[46] H. Hasimoto, "On the periodic fundamental solution of the Stokes equations and their application to viscous flow past a cubic array of spheres," J. Fluid Mech. **5**, 317 (1959).

[47] M. Deserno and C. Holm, "How to mesh up Ewald sums. I. A theoretical and numerical comparison of various particle mesh routines," J. Chem. Phys. **109**, 7678 (1998).

[48] D. Chehata Gómez, L. Bergougnoux, E. Guazzelli, and J. Hinch, "Spreading fronts in sedimentation of dilute suspensions of spheres," Phys. Fluids **20**, 023302 (2008).

[49] B. Metzger, J. E. Butler, and E. Guazzelli, "On wavelength selection by stratification in the instability of settling fibers," Phys. Fluids **19**, 098105 (2007).